A Robust Design Strategy for Resonant Controllers Tuned Beyond the *LCL* filter Resonance Frequency

Xin Zhao, Zhen Kang, Xuanlyu Wu, Weilin Li, Xiaohua Wu
School of Automation
Northwestern Polytechnical University
Xi'an, China
{xzh, kangzhen, wu, liweilin907, wxh}@nwpu.edu.cn

Chuan Xie
School of Automation Engineering
University of Electronic Science and Technology of China
Chengdu, China
c.xie@uestc.edu.cn

Josep M. Guerrero
Department of Energy Technology
Aalborg University, Denmark
joz@et.aau.dkline

***Abstract*—LCL filter is one of the most prevailing approaches for harmonic filtering due to its premium switching order harmonic attenuation performance. However, resonance issues, which may cause system instability, are also induced by the *LCL* filter. Thus, bandwidth of the inner current loop is required to be sufficiently lower than the filter resonance frequency to ensure system stability. In this paper, a robust resonant controller design strategy for converters with *LCL* filters is proposed to enhance the harmonic control capability. With the proposed design method, it is possible to tune the central frequency of the resonant controller above the *LCL* filter resonance frequency without triggering instability issues. In contrast with conventional techniques, the *LCL* filter can be designed with lower resonance frequency by utilizing the proposed approach. This way, a better switching order harmonic attenuation can be achieved without sacrificing high order harmonic tracking capability. Experimental results are presented to demonstrate the effectiveness of the proposed design strategy.**

***Keywords*—LCL filter, resonant controller, control bandwidth, harmonic control capability**

I. INTRODUCTION

Generally, pulse width modulation (PWM) is adopted to drive the converter. However, high order harmonics, especially the switching order harmonics, also appear and may pollute the power grid. Thus, *LCL* filter is usually implemented between the converter and the grid to attenuate the high frequency harmonics produced by the converter [1]. However, along with the advantages that *LCL* filter brought, the well-known resonance issues are also induced into the system and thus make the controller design more challenging [2].

In previous works, various *LCL* filter and control loop design strategies are proposed by researchers. In [3], the influence of system delays on the capacitor current feedback active damping is investigated. In [4], a reduced order system is obtained by splitting the filter capacitor into two parts, and thus achieving high current quality and system stability. By adopting those strategies, an output current with low total harmonic distortion (THD) can be obtained. However, all these control strategies solely discussed the fundamental current tracking, where the current control loop bandwidth is usually set to be far below the filter resonance frequency. Thus, the performance of high order harmonic rejection or injection is degraded due to this low bandwidth. By delicately design the *LCL* filter parameters, a shunt active power filter (SAPF) is designed in [5] and [6] to effectively compensate high order harmonic currents without triggering system instability issues. In [7], a repetitive control based multifunctional grid-connected converter with LCL filter is proposed to simultaneously inject fundamental and harmonic current to the distribution grid, while in [8], a virtual RC damper based harmonic compensation scheme is proposed to provide high quality current to the grid.

Regardless which *LCL* filter and controller design strategy are adopted, the harmonic controller is always required to be tuned below the filter resonance frequency to ensure the system stability. As a consequence, harmonic frequencies adjacent to or higher than the resonance frequency cannot be compensated which is not desirable in applications where the *LCL* filter resonance frequency is low.

In light of the above mentioned issues, it is proved in this paper that central frequency of the resonant controller can be tuned above the filter resonance frequency without triggering instability issues. Consequently, high order harmonics can be suppressed which leaves the grid current with improved power quality. The rest of the paper is organized as follows. Section II gives a detailed analysis regarding the conventional controller design method while Section III illustrates the proposed controller design strategy. Experimental results are analyzed and discussed in Section IV. Finally, Section V presents the conclusion of the paper.

II. CONVENTIONAL CONTROLLER DESIGN STRATEGY

The system under study is shown in Fig. 1, which is a general case of *LCL* filter based grid-connected system. The grid is modeled by an ideal sinusoidal voltage source in series with grid impedance Z_g. L_1, L_2 and C_f denote the converter side inductor, grid side inductor, and filter capacitor, respectively, while v_c, i_L, and v_g denote the capacitor voltage, converter output current, and grid voltage, respectively. Capacitor current feedback based active damping is utilized to address the *LCL* filter resonance issue, and the inner loop controller $G_c(s)$ employs a PR controller to regulate the output current i_g.

Fig. 2 shows the block diagram of the inner control loop in z-domain. The corresponding z-domain plant transfer functions are derived as:

$$G_{mc}(z)=\frac{i_c(z)}{v_m(z)}=\frac{\sin(\omega_{res}T_s)[z^{-1}-z^{-2}]}{\omega_{res}L[1-2z^{-1}\cos(\omega_{res}T_s)+z^{-2}]} \quad (1)$$

$$G_{cg}(z)=\frac{i_g(z)}{i_c(z)}=\frac{T_s^2z^{-1}}{L_gC_f(1-z^{-1})^2} \quad (2)$$

Where $\omega_{res}=\sqrt{(L_1+L_2)/(L_1L_2C_f)}$ is the resonance angular frequency, T_s is the sampling period. Notre that $G_{mc}(z)$ and

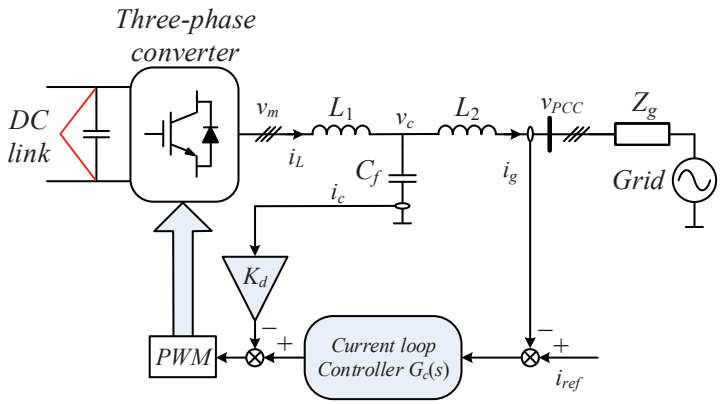

Fig. 1. Three phase converter connected to the grid through a *LCL* filter.

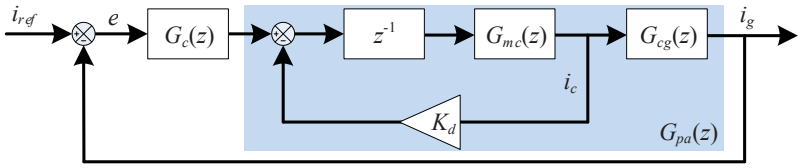

Fig. 2. Plant model.

$G_{cg}(z)$, which stand for the transfer function of converter output voltage to capacitor current and capacitor current to grid current, respectively, are discretized from their corresponding s-domain transfer functions via ZOH method to reflect the PWM delay.

Conventionally, PR controller with phase compensation [9]–[10] can be utilized as the current regulator:

$$G_c(z) = k_p + \sum_{h=1}^{n} k_{Ih} T_s \frac{\cos\varphi_c - z^{-1}\cos\left(\varphi_{ch} - h\omega_f T_s\right)}{1 - 2z^{-1}\cos\left(h\omega_f T_s\right) + z^{-2}} \quad (3)$$

where n denotes the highest harmonic order that can be compensated, h denotes the harmonic order that need to be compensated, φ_{ch} is the phase leading angle, k_p and k_{Ih} are the proportional and the integral gains, respectively.

Since design criteria of the active damping compensator and fundamental PR controller are already well presented in previous publications[11]–[13], they will not be discussed in this paper. The system parameters used both in the analysis and the experiments are listed in Table I, while the tuned inner control loop parameters are directly listed in Table □.

Apart from fundamental current tracking, THD of the grid current is usually required to be less than 5% [14] even with distorted grid voltage. In other applications, such as APF, the converter is controlled to inject harmonic currents to improve the grid current quality. In either harmonic current injection or rejection applications, multiple resonant controllers are adopted to provide high gains at desired frequencies. Conventionally, the value of $n\omega_f$ in (3) is required to be sufficiently lower than ω_{res} to avoid instability issues caused by the filter resonance. To address this issue, open loop transfer function of the system is derived as:

$$G_{ol}(z) = G_c(z)G_{pa}(z) = G_c(z)\cdot\frac{z^{-1}G_{mc}(z)G_{cg}(z)}{1 + z^{-1}K_d G_{mc}(z)} \quad (4)$$

where $G_{pa}(z)$ is the plant model and $G_c(z)$ is the current loop controller that regulates both fundamental and harmonic current. Normally, phase leading angle φ_{ch} is tuned equal with the inverse of the system phase angle [10] to achieve high compensation accuracy and stability margin, i.e., $\varphi_{ch} = -\arg[G_{pa}(z)]\,|\,z = e^{jh\omega_f}$.

Considering that $G_{pa}(jh\omega_f)$ is a function of system damping ratio ξ(i.e., K_d), the relationship between ξ and φ_{ch} is plotted in Fig. 3 for different harmonic frequencies. From Fig. 3, it can be found that the damping ratio has different influences on the phase leading angles at different harmonic frequencies. For the harmonics with frequency lower than ω_{res}, the changing trend of leading angles versus damping ratio tends to increase. Meanwhile, the trend becomes opposite for the harmonics with frequency higher than ω_{res}.

In the conventional controller design method, ξ is selected before designing resonant controllers. Thus, the system phase delay is fixed and φ_{ch} can be obtained directly from $\varphi_{ch} = -\arg[G_{pa}(z)]\,|\,z = e^{jh\omega_f}$. Under this condition, the influence of different ξ on φ_{ch} and the system stability margin is neglected. Thus, to enhance the system stability and harmonic controllability, the influence of ξ on φ_{ch} on system stability should be analyzed, and it is found that by properly coordinating ξ on φ_{ch}, it is possible to control high order harmonics even if its frequency is higher than ω_{res}.

III. Proposed Controller Design Strategy

A. Active damping gain design

Sensitivity function $S(z)$ [15] is utilized to measure the stability margin, since it can give an accurate measurement of system stability margin. Firstly, the influence of damping ratio on system stability margin is evaluated through the Nyquist curve of $G_{pa}(z)$ shown in Fig. 4. The dashed line shows the system without resonant controller while the solid line represents the system with 17th order resonant controller implemented. It can be seen that with the increase of frequency, the distance from the origin to the dashed curve (magnitude of the system transfer function) first decreases until the local minima at frequency f_1, then begins to increase and reaches the local maxima at frequency f_2. After

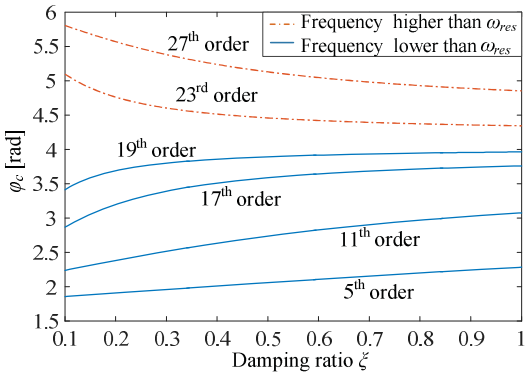

Fig. 3. Relationship between ξ and φ_{ch} at different harmonic frequencies.

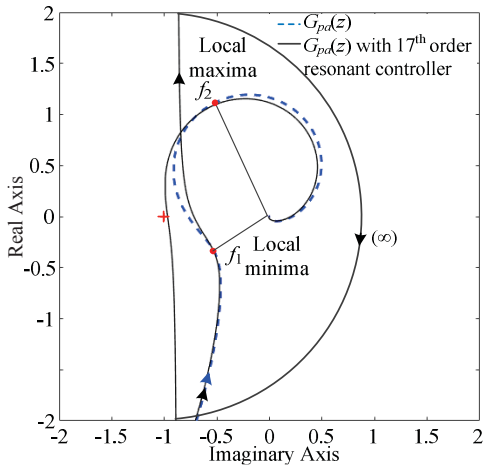

Fig. 4. Nyquist diagram of the open loop system with and without 17th order resonant controller.

implementing the resonant controller, which central frequency locates between f_1 and f_2, the solid curve approaches infinite as shown in Fig. 4. This is due to resonant controller magnitude increases to infinity, and the phase angle shifts 180° clockwise abruptly. Apparently, due to the monotonically increasing characteristic of the magnitude of $G_{pa}(z)$ between f_1 and f_2, the infinite magnitude and 180° phase shift induced by the resonant controller will drive the system Nyquist curve approaching the critical point, finally leading to the decreasing of system stability margin. To avoid the system stability margin from being degraded when implementing high order resonant controllers, the lower boundary of the damping ratio should be designed to turn the magnitude of the system, $|G_{pa}(z)|$, into a monotonically decreasing function. Therefore, the constraint of ξ can be derived as:

$$\frac{\partial \left| G_{pa}(\omega, \xi) \right|}{\partial \omega} < 0 \tag{5}$$

B. Phase leading angle optimization

In this section, phase leading angle is designed to maximize the stability margin of an *LCL* filtered converter whose objective is to compensate up to 23rd order harmonic current with the specifications shown in Table I. According to the analysis presented in section III B, system damping ratio ξ is chosen as 0.4, with a calculated K_d = 9. Then,

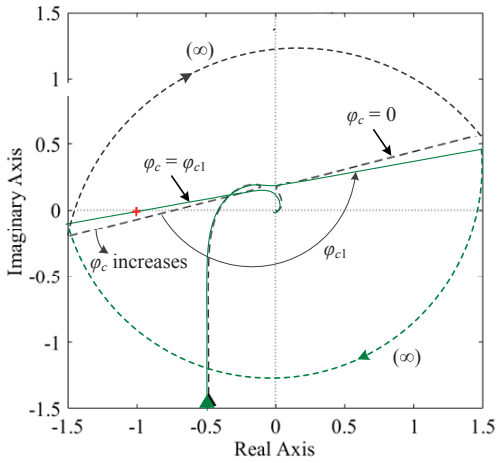

Fig. 5. Nyquist diagram of $G_{ol}(z)$ with different phase leading angles.

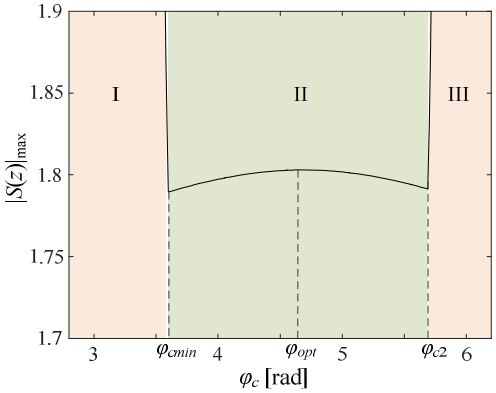

Fig. 6. $|S(z)|$max as a function of φ_c.

TABLE I PARAMETERS OF POWER STAGE

Parameters	*Symbol*	*Value*
Converter Side Inductors	L_1	1.8 *mH*
Grid Side Inductors	L_2	1.8 *mH*
Capacitors	C_f	27 *μF*
LCL Filter Resonance Frequency	f_{res}	1.02 *kHz*
Nominal Voltage	V	230 *V*
Nominal Frequency	ω_f	314 *Rad*
DC Voltage	V_{DC}	650 *V*
Switching Frequency	f_s	10 *kHz*

TABLE □ PARAMETERS OF INNER CONTROL LOOP

Parameters	*Symbol*	*Value*
Proportional gain	k_p	5
Fundamental integral gain	k_{I1}	200
Sampling period	T_s	100 *μs*

sensitivity function is utilized to measure the system stability margin, and a generalized design guideline is provided in detail to illustrate how to maximize the system stability margin. Considering that resonant controller barely affects the system frequency characteristic outside its resonance frequency, thus phase leading angle at each harmonic frequency can be designed individually. Nyquist diagram of $G_{ol}(z)$, which contains one resonant controller tuned at any interested harmonic order, is shown in Fig. 5 with different phase leading angles. Fig. 5 indicates that when φ_c = 0, the critical point is encircled by the Nyquist curve (dashed line).

As φ_c increases from 0 to φ_{c1} , the curve rotates counterclockwise, and goes through the critical point (solid line). When φ_c keeps increasing from φ_{c1} 1 to 2π, the critical point will no longer be encircled which indicates the system enters the stable region. Note that the system stability margin (represented by $|S(z)|$) also changes as φ_c increases.

Thus, to analyze the influence of phase leading angle on system stability margin, $|S(z)|_{max}$ of the system shown in Fig. 5 is plotted in Fig. 6 as a function of phase leading angle. Note that the infinite value of $|S(z)|_{max}$ indicates the Nyquist curve goes through the critical point. Based on Fig. 5, it can be concluded that in order to achieve a stable system, the value of φ_c should be limited in the range of φ_{c1} and 2π. This stable region contains three stages of $|S(z)|_{max}$ variation as shown in Fig. 6. The sharp decrease of $|S(z)|_{max}$ in stage I (between φ_{c1} and φ_{cmin}) is caused by the Nyquist curve rotates away from the critical point. In stage II (between φ_{cmin} and φ_{c2}), $|S(z)|_{max}$ remains relatively stable. Afterwards, the Nyquist curve rotates towards the critical point in stage III (between φ_{c2} and 2π), and the value of $|S(z)|_{max}$ will increase significantly as illustrated in Fig. 6.

Conventionally, the leading angle is set equal to the system delay to achieve high compensation accuracy. However, in high frequency applications, stability issue is more critical than compensation accuracy. Therefore, the leading angle is determined to maximize the system stability margin. As shown in Fig. 6, minimum value of $|S(z)|_{max}$ can be achieved at φ_{cmin}, however, since φ_{cmin} is close to φ_{c1}, the system has a high chance to enter the unstable region in terms of parameters drift. Therefore, the average value of φcmin and φ_{c2} is set as the optimized leading angle φ_{opt}, since it lies in the middle of stage II and thus can provide sufficient stability margin.

IV. Experimental Results

In order to validate the proposed control strategy, experimental study is conducted and the results are included below. The experimental setup is shown in Fig. 7. One converter (2.2kW) is used to emulate the current-controlled converter while the other converter is used to emulate the grid. Specifications of the setup are listed in Tables I and II.

Performance of the controller is validated under a highly distorted grid whose voltage waveform is shown in Fig. 8. Note the grid voltage contains harmonic voltages up to 23rd order which is higher than the *LCL* filter resonance frequency.

For converter embedded with controller designed in the conventional way, 19th and 23rd order harmonics cannot be compensated since they are in the vicinity of the *LCL* filter resonance frequency. As shown in Fig. 9, sizeable high order harmonics appear on the grid current. However, THD of the grid current still maintains at a relatively low level (2.1%) since low order harmonics are well compensated.

Figs. 10 and 11 shows the grid current and its spectrum with all the harmonics compensated under two sets of grid impedance (L_g = 0 and L_g = 8 mH). As it can be seen, grid current becomes sinusoidal after 19th and 23rd order harmonics are compensated. As illustrated in Fig. 11, even though the grid impedance increases from 0 to 8mH, the system is still stable, showing its high robustness in front of large range grid impedance variations.

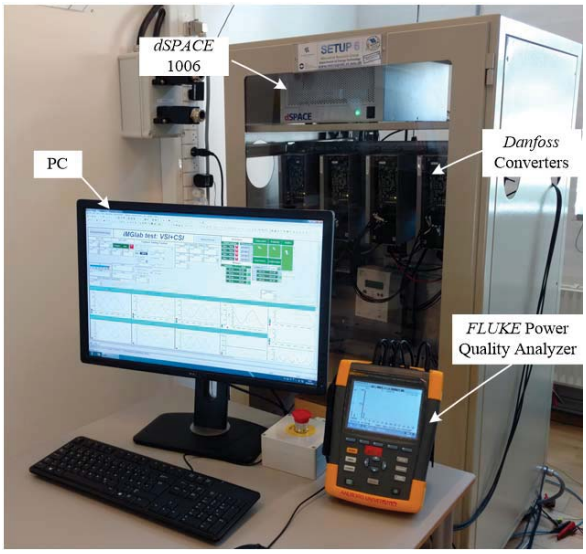

Fig. 7. Experimental setup.

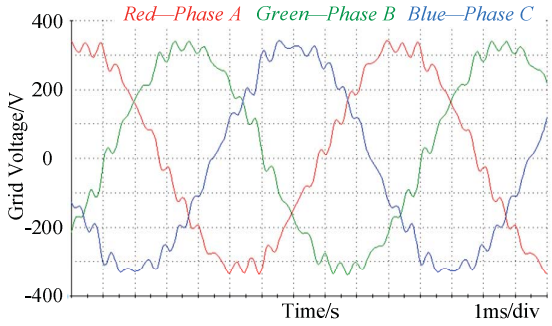

Fig. 8. Grid Voltage.

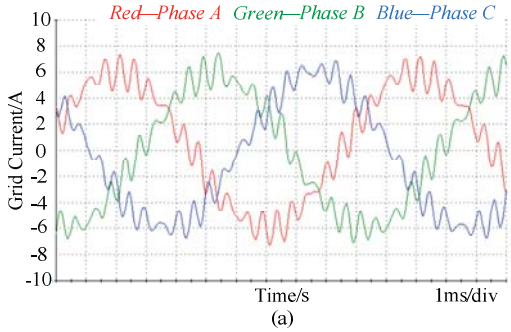

Fig. 9. Grid current with conventional controller design strategy.

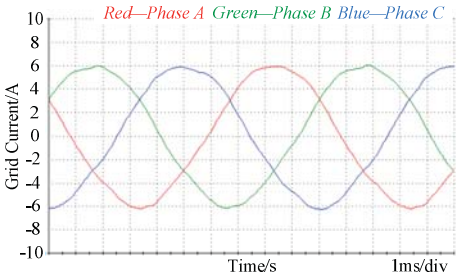

Fig. 10. Grid current with proposed controller design strategy (L_g=0mH).

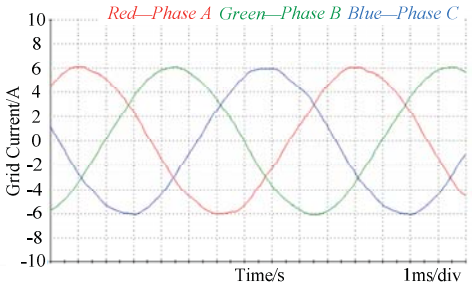

Fig. 11. Grid current with proposed controller design strategy(L_g=8mH).

V. CONCLUSION

In this paper, a robust controller design strategy for *LCL* filter based grid-connected converters is proposed to enhance the harmonic control capability. By coordinating the system damping ratio and the phase leading angle induced by resonant controller, central frequency of the resonant controllers can be tuned above the *LCL* filter resonance frequency, in turn a flexible filter resonance frequency placement can be achieved without compromising high order harmonic control capabilities. Finally, experiments with resonant controller whose central frequency is 350Hz higher than the *LCL* filter resonance frequency validate the theoretical analysis.

REFERENCES

[1] J. Wang, J. D. Yan, L. Jiang, and J. Zou, "Delay-Dependent Stability of Single-Loop Controlled Grid-Connected Inverters with LCL Filters," IEEE Trans. Power Electron., vol. 31, no. 1, pp. 743–757, Jan. 2016.

[2] X. Wang, F. Blaabjerg, and P. C. Loh, "Virtual RC Damping of LCL-Filtered Voltage Source Converters with Extended Selective Harmonic Compensation," IEEE Trans. Power Electron., vol. 30, no. 9, pp. 4726–4737, Sept. 2015.

[3] D. Pan, X. Ruan, C. Bao, and W. Wang, "Capacitor-Current-Feedback Active Damping with Reduced Computation Delay for Improving Robustness of LCL-Type Grid-Connected Inverter," IEEE Trans. Power Electron., vol. 29, no. 7, pp. 3414–3427, Jul. 2014.

[4] G. Shen, D. Xu, L. Cao and X. Zhu, "An Improved Control Strategy for Grid-Connected Voltage Source Inverters With an LCL Filter," IEEE Trans. Power Electron., vol. 23, no. 4, pp. 1899–1906, Jul. 2008.

[5] Y. Tang, P. C. Loh, P. Wang, F. H. Choo, F. Gao and F. Blaabjerg, "Generalized Design of High Performance Shunt Active Power Filter With Output LCL Filter," IEEE Trans. Ind. Electron., vol. 59, no. 3, pp. 1443–1452, Mar. 2012.

[6] Q. Liu, L. Peng, Y. Kang, S. Tang, D. Wu and Y. Qi, "A Novel Design and Optimization Method of an LCL Filter for a Shunt Active Power Filter," IEEE Trans. Ind. Electron., vol. 61, no. 8, pp. 4000–4010, Aug. 2014.

[7] Z. Zou, Z. Wang and M. Cheng, "Modeling, Analysis, and Design of Multifunction Grid-Interfaced Inverters With Output LCL Filter," IEEE Trans. Power Electron., vol. 29, no. 7, pp. 3830–3839, Jul. 2014.

[8] X. Wang, F. Blaabjerg, and P. C. Loh, "Virtual RC Damping of LCL-Filtered Voltage Source Converters with Extended Selective Harmonic Compensation," IEEE Trans. Power Electron., vol. 30, no. 9, pp. 4726–4737, Sept. 2015.

[9] R. I. Bojoi, G. Griva, V. Bostan, M. Guerriero, F. Farina, and F. Profumo, "Current control strategy for power conditioners using sinusoidal signal integrators in synchronous reference frame," *IEEE Trans. Power Electron*., vol. 20, no. 6, pp. 1402–1412, Nov. 2005.

[10] A. G. Yepes, F. D. Freijedo, O Lopez, and J. Doval-Gandoy, "Analysis and Design of Resonant Current Controllers for Voltage-Source Converters by Means of Nyquist Diagrams and Sensitivity Function," IEEE Trans. Ind. Electron., vol. 58, no. 11, pp. 5231–5250, Nov. 2011.

[11] D. G. Holmes, T. A. Lipo, B. P. McGrath, and W. Y. Kong, "Optimized Design of Stationary Frame Three Phase AC Current Regulators," *IEEE Trans. Power Electron*., vol. 24, no. 11, pp. 2417–2426, Nov. 2009.

[12] M. Liserre, F. Blaabjerg, and S. Hansen, "Design and control of an LCL-filter-based three-phase active rectifier," IEEE Trans. Ind. Appl., vol. 41, no. 5, pp. 1281–1291, Sept.-Oct. 2005.

[13] A. Kuperman, "Proportional-Resonant Current Controllers Design Based on Desired Transient Performance," IEEE Trans. Power Electron., vol. 30, no. 10, pp. 5341–5345, Oct. 2015.

[14] IEEE Standard for Interconnecting Distributed Resources with Electric Power Systems, IEEE Standard 1547, 2003.

[15] G. F. Franklin, J. D. Powell and M. L. Workman, Digital Control of Dynamic Systems. Addison-Wesley, 1997.